

Tailoring the magnetic anisotropy of CoFeB/MgO stacks onto W with a Ta buffer layer

Andreas Kaidatzis,^{1,a)} Cristina Bran,² Vasilios Psycharis,¹ Manuel Vázquez,² José Miguel García-Martín,³ and Dimitrios Niarchos¹

¹*Institute of Nanoscience and Nanotechnology, NCSR Demokritos, Aghia Paraskevi, Attikis, Athens 15310, Greece*

²*ICMM-Instituto de Ciencia de Materiales (CNM-CSIC), Sor Juana Inés de la Cruz 3, Cantoblanco, E-28049 Madrid, Spain*

³*IMM-Instituto de Microelectrónica de Madrid (CNM-CSIC), Isaac Newton 8, PTM, E-28760 Tres Cantos, Madrid, Spain*

(Received 30 April 2015; accepted 19 June 2015; published online 29 June 2015)

The emergence of perpendicular magnetic anisotropy (PMA) in CoFeB/MgO stacks deposited on W using a Ta buffer layer is studied as a function of Ta and CoFeB layer thickness and annealing temperature. It is shown that very thin Ta “dusting” layers (thickness between 0.3 and 1 nm) enhance PMA of CoFeB layers grown on top of W. We find that Ta thickness is a crucial factor affecting magnetic anisotropy and it needs to be scaled proportionally to CoFeB thickness for obtaining PMA. Stacks without Ta have in-plane anisotropy, verifying the “PMA-enhancing” role of Ta. The maximum effective PMA energy (3.6×10^6 erg/cm³) is obtained for a stack with 1.4 nm of CoFeB and 1 nm of Ta and after annealing at 350 °C. Besides, PMA can be obtained even at the as-deposited state for certain thicknesses. This W-based CoFeB/MgO system could enable the development of low power consumption, high density, and non-volatile magnetic memories. © 2015 AIP Publishing LLC. [<http://dx.doi.org/10.1063/1.4923272>]

Perpendicular Magnetic Anisotropy (PMA) materials are currently under intense study because of their high potential for use in spintronics applications like Magnetic Random Access Memories (MRAMs),¹ spin-transistors,² and spin-logic devices.³ In particular, Magnetic Tunnel Junctions (MTJs), a stack of two ferromagnetic layers separated by an oxide, are key components of future spintronics technologies. One of the most promising MTJ materials systems is composed of CoFeB/MgO/CoFeB stacks, with PMA arising from the strong CoFeB/MgO interface anisotropy.⁴ These MTJs show high tunnel magnetoresistance and a low threshold current for spin-transfer torque magnetization switching properties of particular importance for MRAM applications. What is more, PMA is a necessary requirement for ensuring high data stability and adequate scalability of the device.

Recently, Spin-Orbit Torque MRAM (SOT-MRAM) has been proposed as a novel memory concept⁵ promising a fast access, energy-efficient, scalable, high density, and non-volatile memory technology. A typical SOT-MRAM stack is composed of a MTJ with PMA, grown on top of a high spin-orbit coupling heavy-metal, which acts as the read/write current line. Although initial SOT-MRAM studies were focused on the Pt/Co/AlO_x system,⁶ there has been a shift towards Ta/CoFeB/MgO structures, due to the higher spin-orbit coupling of Ta, the readily obtainable PMA of CoFeB after annealing and the more effective spin-dependent tunneling through the monocrystalline MgO barrier.⁴

Recent SOT-MRAM studies have been focused on W, for use as current line metal, due to its reported giant spin-orbit interaction⁷ that allows the fabrication of even lower read/write current SOT-MRAM cells, enabling the industrial

application of SOT-MRAM technology. Thus, obtaining W/CoFeB/MgO stacks with good PMA is a hot topic in this field. For instance, Hao and Xiao⁸ perform annealing at 280 °C under a perpendicular magnetic field of 0.45 T, i.e., with high energy consumption, for obtaining PMA. On the other hand, Torrejon and co-workers⁹ anneal their stacks at 300 °C without magnetic field, obtaining PMA when the W layers have thickness of 4 nm or less, but with a reduced CoFeB magnetization, while in-plane anisotropy (IPA) is obtained for 6 nm W thickness. Finally, Pai and collaborators¹⁰ have shown that strong PMA may be obtained only by inserting a thin Hf layer between the W and CoFeB layers.

In a similar context, we study W-based CoFeB/MgO half-MTJ stacks (only the “free” MTJ layer is present), with a configuration in-between the ones mentioned above: we use a 6 nm thick W underlayer, which maintains a high CoFeB magnetization, but with an additional Ta “dusting” layer inserted between W and CoFeB, whose thickness is systematically varied. It is shown that for certain parameters, PMA can be obtained even without annealing. The CoFeB/MgO stack magnetic anisotropy is studied as a function of Ta layer thickness and annealing temperature, and it is shown that the Ta layer thickness needs to be proportionally scaled with the CoFeB thickness for effectively enhancing PMA. The maximum effective PMA energy (3.6×10^6 erg/cm³) is obtained for the sample with 1.4 nm of CoFeB and 1 nm of Ta, after annealing at 350 °C for an hour.

The samples studied were W(6 nm)/Ta(t_{Ta} nm)/Co₂₀Fe₆₀B₂₀(t_{CoFeB} nm)/MgO(2 nm)/AlO_x(2 nm) multilayers, where $t_{Ta} = 0, 0.3, 0.6, \text{ and } 1$ nm and $t_{CoFeB} = 0.9, 1.2, 1.4, \text{ and } 1.8$ nm. CoFeB films with 20 at. % B are deposited to produce an amorphous as-deposited structure,¹¹ while Co₂₀Fe₆₀B₂₀ is reported¹² to have stronger CoFeB/MgO interface anisotropy than

^{a)}Electronic mail: a.kaidatzis@inn.demokritos.gr

Co₆₀Fe₂₀B₂₀. All the stacks were covered by AlO_x for preventing oxygen diffusion through MgO and into CoFeB.

Ultra-high vacuum (base pressure 1.5×10^{-9} Torr) magnetron sputtering was employed for deposition on monocrystalline Si(100) substrates covered with an amorphous 500 nm thick thermal SiO₂. Direct current (radio frequency) power supply was used for metal (oxide) deposition, at 1.5 W/cm^2 (10 W/cm^2) power density and 3 mTorr Ar working pressure, leading to 0.018 nm/s (0.010 nm/s) deposition rate. The substrates were rotating during deposition for avoiding the emergence of any in-plane magnetic anisotropy axes. After deposition, the samples were annealed for 1 h at 250 °C or 350 °C, in an independent high vacuum chamber (pressure during annealing better than 1×10^{-5} Torr). Selected samples were also annealed at 425 °C for 1 h. The ramp-up rate was 20 °C/min and the films were freely cooled to room temperature in high vacuum before removal.

Magnetic hysteresis cycles have been obtained for all the samples using vibrating sample magnetometry. The magnetic field was applied either in the plane or perpendicular to the plane of the samples. Fig. 1 shows a representative set of hysteresis cycles: the ones of the $t_{\text{CoFeB}} = 1.4 \text{ nm}$ samples series, after annealing at 250 °C. It is clear that the magnetic anisotropy evolves upon change of the Ta layer thickness: low thickness results in IPA, as the easy magnetization axis is in the plane of the sample and large thickness in PMA (the easy magnetization axis is perpendicular to the plane of the sample). The anisotropy field H_k , defined as the hard-axis saturation field and measured at the intersection of the in-plane and perpendicular to the plane loops,¹³ increases from -5.6 kOe for $t_{\text{Ta}} = 0.3 \text{ nm}$ (minus sign indicates IPA, whilst positive indicates PMA) to -0.9 kOe for $t_{\text{Ta}} = 0.6 \text{ nm}$ and 3.4 kOe for $t_{\text{Ta}} = 1 \text{ nm}$.

Similar behavior is observed for $t_{\text{CoFeB}} = 1.2 \text{ nm}$ samples: low t_{Ta} results in IPA and large t_{Ta} (≥ 0.6 in this case) in PMA. In contrast, the $t_{\text{CoFeB}} = 0.9 \text{ nm}$ samples only exhibit PMA for $t_{\text{Ta}} = 0.3 \text{ nm}$. Finally, the $t_{\text{CoFeB}} = 1.8 \text{ nm}$ samples have always IPA for any t_{Ta} and any annealing temperature. All the IPA samples have coercive field, H_c , less than 10 Oe and the PMA samples have H_c between 10 Oe and 30 Oe, with the value increasing as the annealing temperature increases.

For further characterizing our stacks, we determine their magnetization and dead magnetic layer thickness. In order to calculate these values, the magnetic moment per surface area versus t_{CoFeB} has been plotted for every t_{Ta} and annealing temperature (see Fig. 2(a)). Linear fittings to the data yield the M_S from the slope and the dead-layer thickness from the y-axis intercept.

M_S values do not change substantially as t_{Ta} variate. The average M_S value is $1279 \pm 71 \text{ emu/cm}^3$ as-deposited and $1292 \pm 62 \text{ emu/cm}^3$ after annealing at 250 °C. However, there is a small decrease after annealing at 350 °C, as M_S is $1201 \pm 62 \text{ emu/cm}^3$, probably due to the increased inter-layer diffusion. This trend is verified by selected samples annealed at 425 °C: their magnetization decreased down to $370 \pm 33 \text{ emu/cm}^3$ and $830 \pm 38 \text{ emu/cm}^3$ for CoFeB thickness equal to 1.2 nm and 1.4 nm, respectively.

Fig. 3 shows the dead layer thickness values as a function of t_{Ta} and annealing temperature. The overall trend

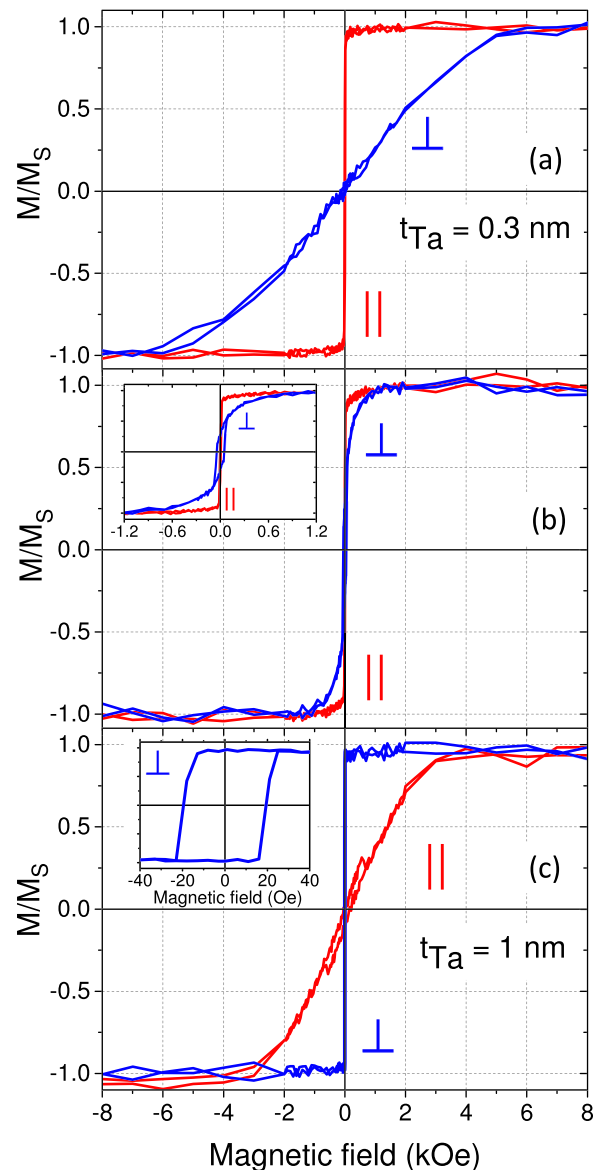


FIG. 1. Representative M-H loops of $t_{\text{CoFeB}} = 1.4 \text{ nm}$ stacks annealed at 250 °C: (a) $t_{\text{Ta}} = 0.3 \text{ nm}$, (b) $t_{\text{Ta}} = 0.6 \text{ nm}$, and (c) $t_{\text{Ta}} = 1 \text{ nm}$. The insets in (b) and (c) show low field regions for clarity.

observed is that the dead-layer thickness is increasing as t_{Ta} increases. Also, there is an increase of the dead-layer thickness after annealing, while it remains rather unchanged when increasing the annealing temperature from 250 °C to 350 °C.

Previous reports show that the dead-layer thickness values depend strongly on the under-layer: CoFeB/MgO stacks deposited on Hf or on W and W/Hf under-layers have almost zero dead-layer thickness.^{10,14} However, CoFeB/MgO stacks have dead-layer thickness ranging from 0.5 to 1.1 nm, when deposited on Ta under-layers.^{12,15} In our stacks, we find a small dead-layer thickness (0.07 nm before annealing up to almost 0.3 nm after annealing at 350 °C) at the CoFeB/MgO stacks deposited directly on W, contrary to previous reports. However, in accordance with the previous studies, it appears that Ta increases the dead-layer thickness reaching a maximum value for $t_{\text{Ta}} = 1 \text{ nm}$: 0.25 nm before annealing and 0.65 nm after annealing at 350 °C.

For investigating the effect of t_{Ta} and annealing temperature on the magnetic anisotropy of the W/Ta/CoFeB/MgO

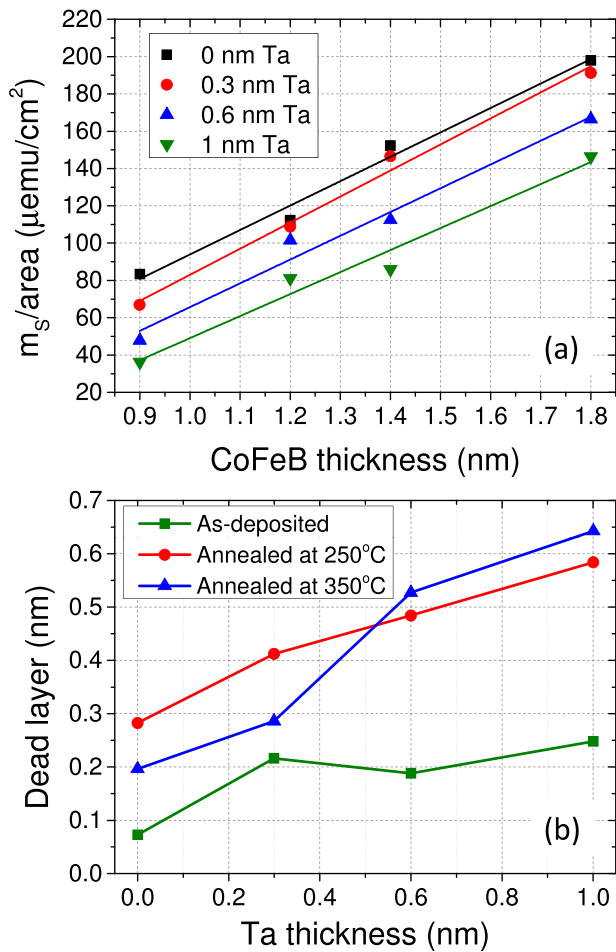


FIG. 2. (a) Representative magnetic moment per surface area versus t_{CoFeB} plot for the samples annealed at 250°C. Solid lines represent linear fits to the data. (b) Dead-layer thickness variation as a function of t_{Ta} and annealing temperature.

system, we determine for each sample its effective magnetic anisotropy energy, K_{eff} (separated in a volume contribution, K_v , and a contribution from the interfaces, K_s), which approximately obeys the relation:¹³

$$K_{\text{eff}} = K_v + \frac{K_s}{t_{\text{CoFeB}}}. \quad (1)$$

As it has been shown,¹⁴ K_s solely originates from the CoFeB/MgO interface, thus, Eq. (1) takes into account only one interface. Finally, K_{eff} is negative (positive) for IPA (PMA) and can be determined experimentally¹³ using the formula $K_{\text{eff}} = H_k M_s / 2$.

Fig. 3 shows the variation of K_{eff} as a function of t_{CoFeB} and t_{Ta} , before and after annealing. Samples with $t_{\text{Ta}} = 0$ have always IPA for any t_{CoFeB} , before and after annealing. Additionally, samples with $t_{\text{CoFeB}} = 1.8$ nm have also IPA, for any Ta thickness, before and after annealing, indicating that this CoFeB thickness is above the threshold where volume anisotropy prevails over the CoFeB/MgO interface anisotropy. Samples with $t_{\text{Ta}} = 0.3$ nm have IPA in all cases, except for $t_{\text{CoFeB}} = 0.9$ nm: in this case, the sample develops PMA after annealing at 250°C, which is sustained even after annealing at 350°C. Finally, samples with $t_{\text{Ta}} = 0.6$ nm or 1 nm have PMA even as-deposited (for $t_{\text{CoFeB}} = 1.2$ nm) and after

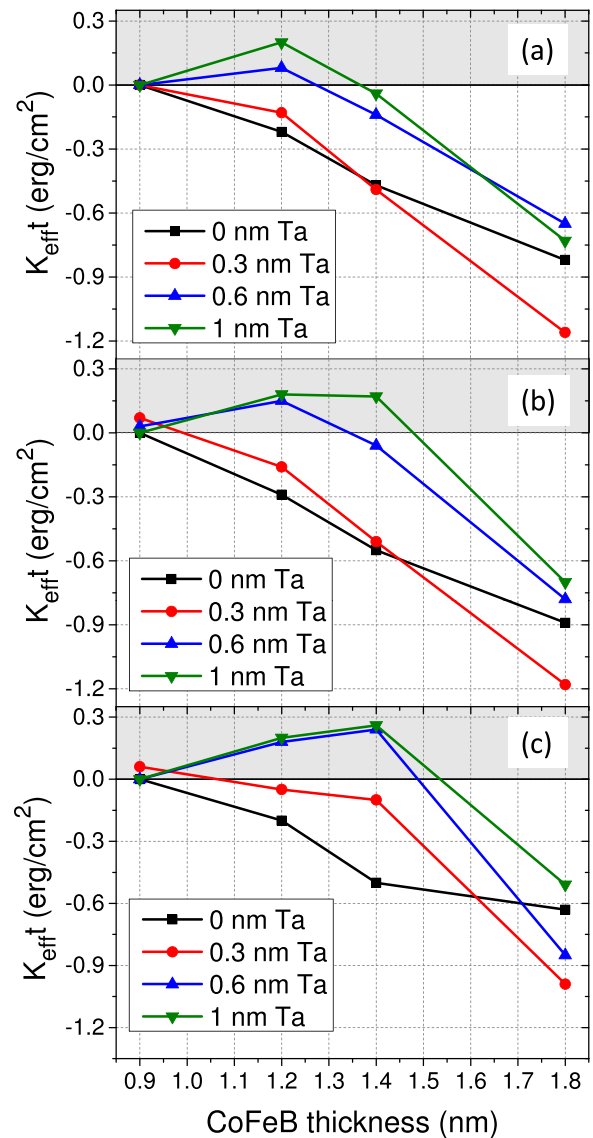


FIG. 3. Effective anisotropy energy K_{eff} as a function of t_{CoFeB} , t_{Ta} , and annealing temperature. As-deposited (a) annealed at 250°C (b) and annealed at 350°C (c) samples. Shaded regions correspond to samples having PMA.

annealing for $t_{\text{CoFeB}} = 1.2$ nm or 1.4 nm, while their PMA energy increases as the annealing temperature increases.

The maximum PMA anisotropy energy, 3.6×10^6 erg/cm³, is obtained for $t_{\text{Ta}} = 1$ nm and $t_{\text{CoFeB}} = 1.4$ nm. This value is slightly smaller than the maximum anisotropy energy measured at W/Hf/CoFeB/MgO samples (4×10^6 erg/cm³ observed for $t_{\text{CoFeB}} = 1.1$ nm)¹⁰ and considerably smaller than the maximum value measured at a Hf/CoFeB/MgO samples (6×10^6 erg/cm³ observed for $t_{\text{CoFeB}} = 1.1$ nm).¹⁴ However, it should be noted that Hf is inadequate material for SOT-MRAM applications due to its low spin-orbit coupling. Finally, the well-studied Ta/CoFeB/MgO system is reported to have values between 1.8×10^6 erg/cm³ and 4×10^6 erg/cm³, both for $t_{\text{CoFeB}} = 0.9$ nm.^{12,14} The obtained maximum anisotropy energy value in addition to the fact that our W/Ta/CoFeB/MgO stacks retain their high spin-orbit coupling β -W phase⁷ even after annealing at 350°C for 1 h,¹⁶ make this system highly promising for SOT-MRAM applications. It is worth mentioning that higher annealing temperature does not improve the PMA anisotropy energy:

samples annealed at 425 °C have almost zero anisotropy. Besides, CoFeB/MgO PMA stacks have been reported to have thermal endurance up to 425 °C only when deposited on Mo underlayers.¹⁷

Our data show that the overall effect of post-deposition annealing is to enhance PMA, up to 350 °C, in contrast to previous studies reporting that PMA is destroyed at this temperature.^{12,18} For explaining this disagreement, the exact role of Ta has to be taken into account. As-deposited amorphous CoFeB layer crystallizes upon annealing in body-centered-cubic (001) structure, coherently to the MgO (001) layer, giving rise to high interface anisotropy.¹¹ In this process, Ta acts as an efficient B getter, enhancing B out-diffusion and allowing for crystallization to occur. Spectroscopic studies have shown that B piles-up at the Ta/CoFeB interface creating a layer of Ta-B mixture.¹⁹ However, excessive annealing results in Ta diffusion into the CoFeB layer and up to the CoFeB/MgO interface,²⁰ which deteriorates the CoFeB (001) orientation, decreases the CoFeB/MgO interface anisotropy, and ultimately destroys PMA.

In our study, all the samples exhibiting PMA show a steady increase of PMA energy after annealing and as the annealing temperature increases from 250 °C to 350 °C. This could be explained on the basis of the extent of Ta doping: when the Ta inter-layer has an optimum thickness, it provides sufficient Ta atoms for assisting B out-diffusion from CoFeB, while keeping Ta diffusion into CoFeB minimum. That is why the dead layer thickness increases after annealing, while M_s remains almost constant. In effect, Ta doping is tailored instead of depositing the CoFeB/MgO stack on top of a pure-Ta under-layer, which acts as a constant source of Ta atoms. This also indicates that W diffusion into CoFeB is poor, as no PMA deterioration is observed upon annealing. Finally, the fact that stacks with no Ta layer have always IPA indicates that the CoFeB layer remains amorphous after annealing, probably because W is a poor B getter. The above point to the fact that there is a favorable window of CoFeB/Ta ratios which results in PMA of the W/Ta/CoFeB/MgO stacks. Below this range, the CoFeB layer insufficiently crystallizes; while above, there is an excessive Ta diffusion into CoFeB. In both cases, IPA is observed.

To conclude, we have demonstrated the importance of Ta doping for obtaining W/CoFeB/MgO stacks with PMA. The extent of Ta doping is the primary parameter affecting CoFeB magnetic anisotropy. There is a window of Ta/CoFeB ratio

where PMA may emerge. Below this range, Ta is insufficient for inducing CoFeB crystallization and therefore PMA. Above this range, excessive Ta diffusion into CoFeB destroys PMA.

Funding from the E.C. through a FP7-ICT project (Grant No. 318144) and CSIC (Ref. i-LINK0783) was acknowledged. Stimulating discussions with Dr. Gilles Gaudin from Spintec, CNRS, France and Professor Pietro Gambardella from ETH, Switzerland are acknowledged.

- ¹R. Sbiaa, H. Meng, and S. N. Piramanayagam, *Phys. Status Solidi RRL* **5**, 413 (2011).
- ²S. Sugahara and J. Nitta, *Proc. IEEE* **98**, 2124 (2010).
- ³M. Becherer, G. Csaba, W. Porod, R. Emling, P. Lugli, and D. Schmitt-Landsiedel, *IEEE Trans. Nanotechnol.* **7**, 316 (2008).
- ⁴S. Ikeda, K. Miura, H. Yamamoto, K. Mizunuma, H. D. Gan, M. Endo, S. Kanai, J. Hayakawa, F. Matsukura, and H. Ohno, *Nat. Mater.* **9**, 721 (2010).
- ⁵I. M. Miron, K. Garello, G. Gaudin, P.-J. Zermatten, M. V. Costache, S. Auffret, S. Bandiera, B. Rodmacq, A. Schuhl, and P. Gambardella, *Nature* **476**, 189 (2011).
- ⁶I. M. Miron, G. Gaudin, S. Auffret, B. Rodmacq, A. Schuhl, S. Pizzini, J. Vogel, and P. Gambardella, *Nat. Mater.* **9**, 230 (2010).
- ⁷C.-F. Pai, L. Liu, Y. Li, H. W. Tseng, D. C. Ralph, and R. A. Buhrman, *Appl. Phys. Lett.* **101**, 122404 (2012).
- ⁸Q. Hao and G. Xiao, *Phys. Rev. Appl.* **3**, 034009 (2015).
- ⁹J. Torrejon, J. Kim, J. Sinha, S. Mitani, M. Hayashi, M. Yamanouchi, and H. Ohno, *Nat. Commun.* **5**, 4655 (2014).
- ¹⁰C.-F. Pai, M.-H. Nguyen, C. Belvin, L. V.-Leao, D. C. Ralph, and R. A. Buhrman, *Appl. Phys. Lett.* **104**, 082407 (2014).
- ¹¹S. Yuasa and D. D. Djayapawira, *J. Phys. D: Appl. Phys.* **40**, R337 (2007).
- ¹²V. Sokalski, M. T. Moneck, E. Yang, and J.-G. Zhu, *Appl. Phys. Lett.* **101**, 072411 (2012).
- ¹³M. T. Johnson, P. J. H. Bloemen, F. J. A. den Broeder, and J. J. de Vries, *Rep. Prog. Phys.* **59**, 1409 (1996).
- ¹⁴T. Liu, J. W. Cai, and L. Sun, *AIP Adv.* **2**, 032151 (2012).
- ¹⁵D. C. Worledge, G. Hu, D. W. Abraham, J. Z. Sun, P. L. Trouilloud, J. Nowak, S. Brown, M. C. Gaidis, E. J. OSullivan, and R. P. Robertazzi, *Appl. Phys. Lett.* **98**, 022501 (2011).
- ¹⁶A. Kaidatzis, V. Psycharis, J. M. García-Martín, C. Bran, M. Vázquez, and D. Niarchos, in *Symposium M – Materials and Technology for Nonvolatile Memories*, edited by P. Dimitrakakis, Y. Fujisaki, G. Hu, and E. Tokumitsu (Mater. Res. Soc. Symp. Proc., 2015), Vol. 1729.
- ¹⁷T. Liu, Y. Zhang, J. W. Cai, and H. Y. Pan, *Sci. Rep.* **4**, 5895 (2014).
- ¹⁸H. Meng, W. H. Lum, R. Sbiaa, S. Y. H. Lua, and H. K. Tan, *J. Appl. Phys.* **110**, 033904 (2011).
- ¹⁹T. Zhu, Y. Yang, R. C. Yu, H. Ambaye, V. Lauter, and J. Q. Xiao, *Appl. Phys. Lett.* **100**, 202406 (2012).
- ²⁰S. Ikeda, J. Hayakawa, Y. Ashizawa, Y. M. Lee, K. Miura, H. Hasegawa, M. Tsunoda, F. Matsukura, and H. Ohno, *Appl. Phys. Lett.* **93**, 082508 (2008).